JOURNAL OF PROPULSION AND POWER
Vol. 18, No. 5, September–October 2002

Study of Flow Separation in Truncated Ideal Contour Nozzle

S. B. Verma*
DLR Lampoldshausen, D-74239 Hardthausen, Germany

An experimental program has been conducted to study the flow separation phenomena in a truncated ideal contour rocket nozzle. Tests indicate that the off-design overexpanded nozzle flow was dominated by shock-induced boundary-layer separation that demonstrated fluctuating characteristics. The separation shock fluctuates back and forth, the intensity of which shows a strong dependence on the nozzle contour. Asymmetry in flow separation was also observed at certain pressure ratios. The study was made using schlieren flow visualization and surface pressure measurements.

Nomenclature

D_e	=	nozzle exit diameter
d^*	=	nozzle throat diameter
F_{SL}	=	side load acting on the nozzle from the gas flow
M_{sep}	=	flow Mach number at separation
P_b	=	back pressure in the vacuum tank
P_{ct}	=	pressure in the charge tube
P_p	=	plateau pressure downstream of separation
P_{sep}	=	wall pressure at separation
P_{st}	=	pressure in the stagnation chamber
P_w	=	local wall pressure
R_{D_e}	=	Reynolds number based on the nozzle exit diameter
$R(x, \phi)$	=	nozzle radius as a function of axial and circumferential coordinate
r_t	=	radius of nozzle throat
T_{tube}	=	temperature in the charge tube
T_0	=	temperature in the stagnation chamber
X	=	coordinate along the nozzle axis (Fig. 10)
X_{MD}	=	distance of the Mach disk from the nozzle exit plane
X_{Md}	=	distance of the Mach disk from the nozzle throat
ϵ	=	area ratio of the nozzle
ϵ_{sep}	=	area ratio of the nozzle at separation
Π	=	nozzle operating pressure ratio
$\sigma_{\max}$	=	maximum value of rms
σ_p	=	rms of the local wall pressure
ϕ	=	circumferential angle (Fig. 10)

Introduction

WITH the start of low area ratio conical nozzles, early developments were focused on large area ratio bell-shaped nozzles. Subsequently, the emphasis turned to improved thrust performance and possible reduction in the nozzle envelope dimensions. In recent years, the emphasis has shifted to space engines and the use of conventional bell nozzles of high area ratio, but of limited length.[1]

In today's launch vehicles, such as the U.S. space shuttle, European Ariane 5, or Titan IVB, the main engines usually operate from takeoff at sea level up to high altitudes with very low ambient pressures. The hot combustion gases from these engines are released using convergent–divergent bell-shaped nozzles to accelerate them to high exit velocities. To get an optimum performance over the whole flight trajectory, the nozzles are designed for an intermediate pressure ratio P_{st}/P_a, at which the exhaust flow is adapted to the ambient pressure P_a. However, this design ambient pressure is chosen high enough to prevent flow separation inside the nozzle during steady-state operation at sea level. Nevertheless, the flow separates from the wall in the divergent part of these nozzles as long as the chamber pressure p_c has not yet reached its nominal operational value.

Flow separation in rocket nozzles is considered undesirable because an asymmetry in the flow separation can cause dangerous lateral forces, the so-called side loads, which may damage the nozzle.[2] The first flight of the Titan IVB launch vehicle with its new solid rocket motor upgrade gave unexpectedly high nozzle actuator loads during ignition.[3] The ensuing effort to define the root cause converged on asymmetrical flow separation in the nozzles. Work in the early 1960s and 1970s produced a number of theories and a large volume of separation data; however, the underlying mechanism behind separation was not totally clear. The computational models developed thus far are close in predicting flow separation, but suffer from a lack of a basic physical justification.

An important factor limiting the performance of a rocket engine are the loads induced by unsymmetrical and unsteady flow separation in the nozzle extension during launch. These operational conditions typically occur during the startup and throttledown processes of a rocket motor at sea level and can cause severe dynamic side loads. Such loads can sometimes be of such a magnitude that they present life-limiting constraints on thrust chamber components, as well as on the thrust vector control system.[4] The primary reason for these loads is the oscillatory nature of the partially detached and partially attached flow at overexpanded conditions. Side loads have been observed during initial startup of overexpanded sea-level liquid propellant rocket engines, as well as during ignition and staging of multistage solid propellant rockets.[4] Because of the severe complications experienced due to too high levels of side loads, they are one of the most important features in sea-level nozzle design.

The traditional design approach for bell-type nozzles is to design the nozzle contour and area ratio in which attached flow and low levels of side loads are guaranteed at nominal operation at high ambient pressure, sea-level conditions. Furthermore the structure is designed robust enough to withstand the side loads during the throttling up and down processes. The reduced performance under vacuum ambient condition and the corresponding weight penalty with a robust design is accepted with this design approach. Increasing demands for improved launcher performance, however, push the development of new concepts. One possible solution is to adapt the nozzle contour during flight to the changes of ambient and chamber pressure. Attempts in this direction, however, have thus far not been successful due to the weight and mechanical complexities of such devices. The main reason why such devices do not exist in full scale is that several basic questions regarding the nature of separation phenomena and the corresponding side loads remain to be answered.

An ideal nozzle has a huge nozzle length, especially because of the last part of the contour with only minor inclination needed

Received 16 November 2001; revision received 28 May 2002; accepted for publication 18 June 2002. Copyright © 2002 by the American Institute of Aeronautics and Astronautics, Inc. All rights reserved. Copies of this paper may be made for personal or internal use, on condition that the copier pay the $10.00 per-copy fee to the Copyright Clearance Center, Inc., 222 Rosewood Drive, Danvers, MA 01923; include the code 0748-4658/02 $10.00 in correspondence with the CCC.

*Research Scientist, Space Propulsion.

to obtain uniform flow. Because of the low wall slopes, the thrust contribution of this end portion is negligible. Therefore, truncation of the last nozzle portion makes this approach feasible for rocket motors, without significant losses in performance because of the nonuniformity of the flow. For example, the Viking and RD-0120 are designed as truncated ideal contour nozzles.[2] The present work is an attempt to study the flow separation characteristics in a truncated ideal contour (TIC) nozzle. The separation shock was observed to exhibit large-scale oscillatory motion, which was found to depend strongly on the separation location inside the nozzle. The flowfield outside the nozzle was studied using in optical schlieren system, whereas the flow inside was investigated using pressure transducers mounted flush on the nozzle contour. Both flow analyzing techniques revealed unsymmetrical movement of the separation point. The area ratio of the TIC nozzle was 20.66, and the Reynolds number range for the tests carried out was $3.298–4.122 \times 10^6$.

Experimental Setup and Procedure

Tests were carried out in the hypersonic wind-tunnel facility at Hyperschall Technologie Göttingen (HTG), which is designed on a completely new concept based on the Ludwieg-tube principle, implementing state-of-art technologies.[5] Figure 1 shows a schematic of the existing wind-tunnel facility at HTG. The tunnel has a test-section diameter of 250 mm and a variable Mach number capability over the range of 6–11 with maximum run time of 100 ms. The high-pressure storage is developed in the form of a long charge tube (30-mm diam) that is interconnected to a vacuum tank through the fast acting valve, the hypersonic nozzle, and the test section.

For the rocket nozzle study, the present test setup had to be modified, as shown in Fig. 2. For this purpose, the conical hypersonic nozzle in the test facility was removed and a stagnation chamber mounted for the nozzle tests. Because the charge tube diameter of the existing wind-tunnel facility is 30 mm and the throat diameter of the TIC nozzle is 20 mm, the area ratio is not sufficient to produce sonic conditions at the throat of the nozzle to accelerate the flow to high Mach numbers. Earlier studies at HTG have shown that for a Mach number range of 6 and below, this problem occurs because of the fixed diameter of charge tube, and so we have to resort to a tandem arrangement of nozzle blocks that help increase the initial diameter of the charge tube to 50 mm. Figure 3 shows the tandem

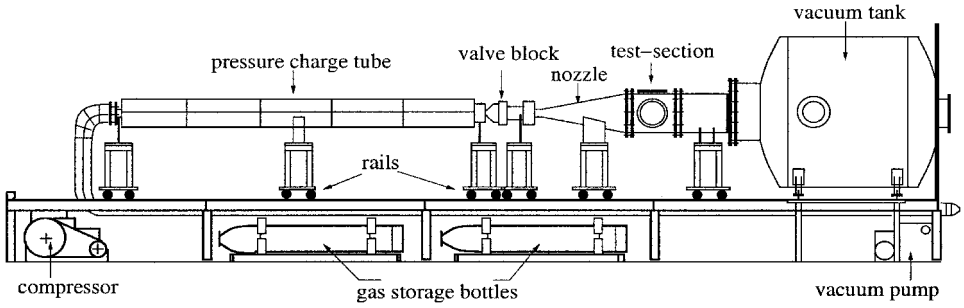

Fig. 1 Schematic of the hypersonic wind-tunnel facility at HTG.

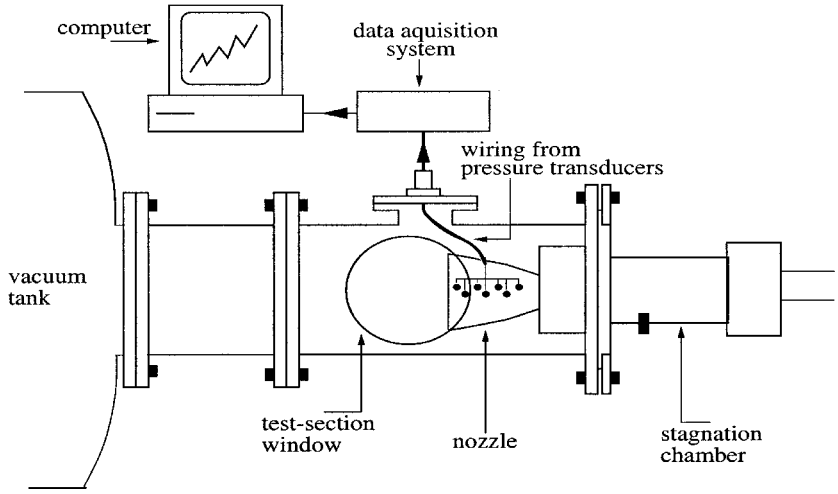

Fig. 2 Modified test setup of the existing facility at HTG.

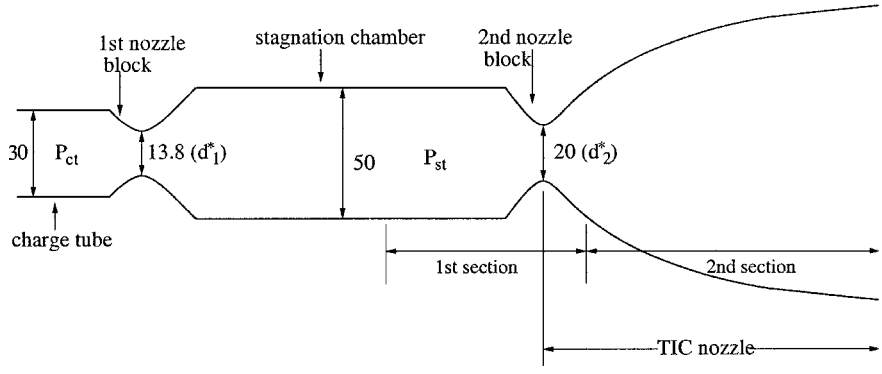

Fig. 3 Tandem arrangement used for nozzle flow study all dimensions in millimeters.

Table 1 TIC nozzle specifications

Parameter	Value
Area ratio	20.66
Design pressure ratio	70
Nozzle throat radius	10 mm
Nozzle exit radius	45.46 mm
Radius of arc in the convergent section	10 mm
Radius of arc in the divergent section	5 mm
Length of nozzle	148.41 mm
Wall inclination at last point of arc	16 deg
Wall inclination at nozzle exit	5.84 deg

arrangement used. To achieve this, an initial nozzle block with a throat diameter of 13.8 mm is placed downstream of the charge tube. This nozzle block opens into a 50-mm tube that now acts as a settling chamber for the second nozzle block. Two flow screens are also placed in this stagnation chamber. The second nozzle block (Fig. 3) has been fabricated in two sections. The first section contains the constant area section, followed by the throat of the nozzle, which was carefully designed to have a shock-free entry into the expansion region. A small portion of the initial nozzle expansion part is also contained in this nozzle block. The remaining and the final expansion part of the TIC nozzle forms the second section. These two sections are joined with the help of an external screw to form a single TIC nozzle. This entire modified section containing the stagnation chamber and TIC nozzle was mounted onto the test section of the original wind tunnel via a flange arrangement. Once this is achieved, the test nozzle can be blown inside the test section with the backpressure, into which the nozzle blows, controlled via a vacuum pump connected to the vacuum tank of the wind tunnel. Table 1 gives the specifications of the TIC nozzle studied. The data for fabrication of the TIC nozzle used for the present study were acquired from DLR Lampoldshausen, where related work on nozzle flow separation had been going on in the past years.

However, stagnation pressure losses occur in such an arrangement. The ratio of the pressures in the charge tube and stagnation chamber can be estimated using the isentropic flow assumption as follows:

The diameter of the two throats involved in this arrangement are

$$d_1^* = 13.8 \text{ mm}, \qquad d_2^* = 20.0 \text{ mm}$$

With the same mass flow passing through the two throats, we have

$$m_1^* = m_2^*$$

and because

$$m_{\max} = \frac{0.6847 P_0 A^*}{\sqrt{RT_0}}$$

we have

$$P_{\text{ct}} A_1^* = P_{\text{st}} A_2^*$$

or,

$$P_{\text{ct}}/P_{\text{st}} = A_2^*/A_1^* = (20/13.8)^2 = 2.1004$$

However, viscous effects in real flow conditions further increase this ratio. Figure 4 shows the plot of time-dependent stagnation pressures during one of the preliminary test runs. The upper curve represents the charge tube pressure and the lower the pressure in the stagnation chamber. Therefore, it can be seen that when steady flow conditions are reached (at approximately 70 ms), a pressure ratio($P_{\text{ct}}/P_{\text{st}}$) of 2.15 is achieved as opposed to 2.1, assuming isentropic flow conditions. This value of pressure ratio also helps to control the stagnation pressure value for different nozzle operating pressure ratios.

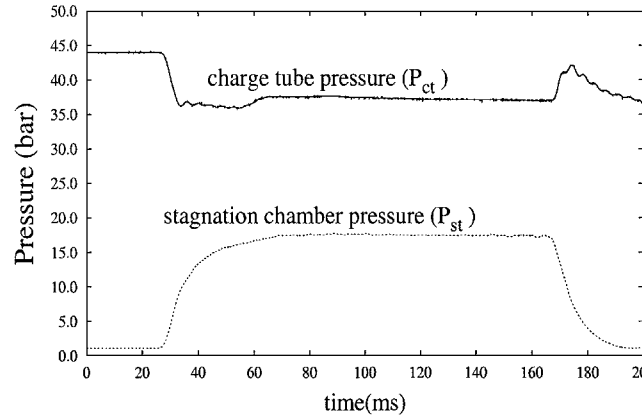

Fig. 4 Time-history of recorded pressure from pressure sensors inside the charge tube and stagnation chamber for rocket nozzle study.

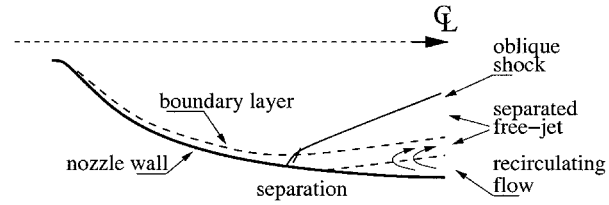

Fig. 5 Free-shock separation in overexpanded rocket nozzles.[2]

Wall Pressure Sensors and Data Acquisition

The pressure transducers used in the nozzle wall pressure experiments are commercially available Sensor Technics SCC series piezoresistive silicon pressure sensor devices (model SCC15AHO). This is an extremely low-cost sensor element with a stable output when driven with a constant current source and designed for use with noncorrosive, nonionic working fluids such as air, dry gases, and the like. They have a pressure-sensitive area 0.15 cm in diameter and an outer case diameter of 0.75 cm. According to the manufacturer's specifications, these transducers have a natural frequency of 10 kHz (0.1-ms response time). They are capable of operating in the temperature range of −40 to +85°C and humidity of 0–100% relative humidity (RH). The accuracy, according to manufacturer's specification, is within 0.5% in the operating pressure range of 0–15 psia. The sensitivity of the transducers is typically 2–6 mV/psi. The transducers were calibrated statically against tank pressure with the zeroing being done under vacuum conditions.

A data acquisition system, which can record 32 channels at a speed of up to 40 kHz, was used to record the measured data. The amplifier that monitors the signal voltage also conditions the signal by amplifying it to the range expected by the A/D converter. The sampling frequency of the signal was 5 kHz. Data stored on hard disk are available for postprocessing and graphical output. Piezoresistive pressure gauges have been calibrated and installed to measure the flow in the charge tube, test section, and vacuum tank. The tests were carried out for operating pressure ratios ranging from 12 to 250. With $T_0/T_{\text{tube}} = 0.955$ and room temperature of 15°C, the Reynolds number based on the nozzle exit diameter (90.92 mm) Re_{De} under the aforementioned test conditions comes out to be in the range of $3.298–4.122 \times 10^6$.

Results and Discussions

Shock Structure Visualization

Of primary importance is the first complete shock cell after the flow inside the nozzle has separated. Subsequent cells are disrupted by shear layers at the boundary and slipstream and vorticity gradients from the shocks; thus, their shock structure is not as sharply defined. Figure 5 shows the type of separation that exists in this class of nozzles. This type of free-shock separation was first reported by Foster et al.[6] (Fig. 5, reproduced from Ref. 2). The separation shock originates at the separation point, but its strength, location, and angle

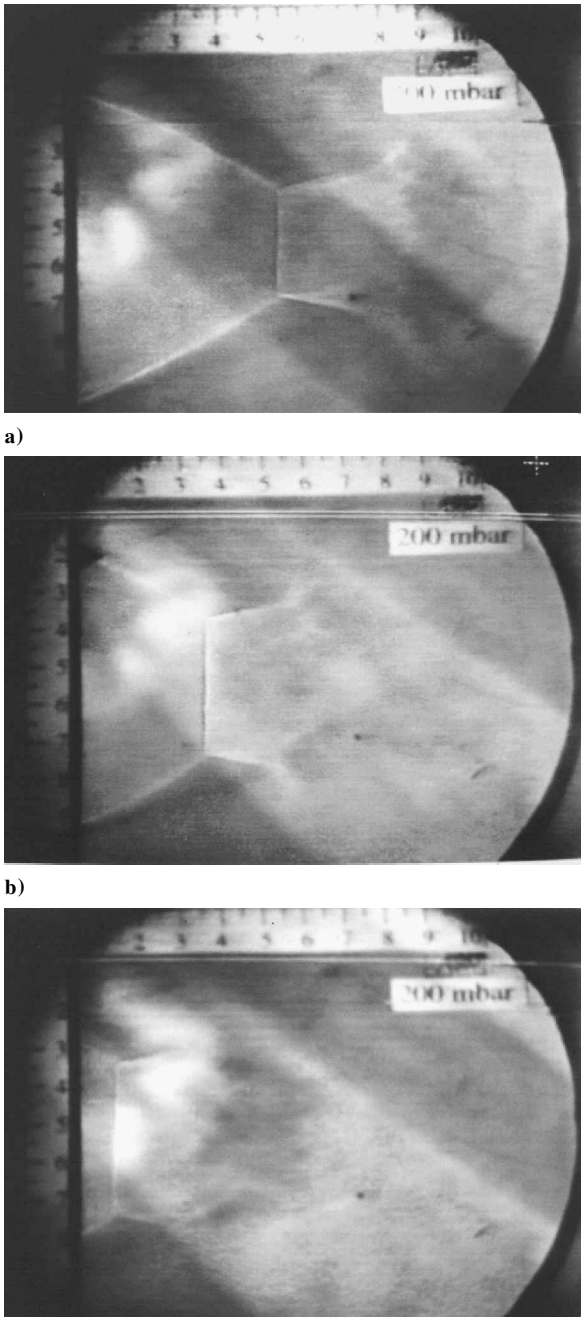

a)

b)

c)

Fig. 6 Schlieren photos of the subscale TIC nozzle during operation at pressure ratio ranging between 50–33 at time instants a) t_1, b) t_2, and c) t_3.

are dictated by the overall adjustment process of the complete first cell. Thus, the shape of the first shock cell reveals a lot regarding the type, nature (symmetric or asymmetric), and location of separation.

Flow exiting from the nozzle is visualized using an optical schlieren system. Figure 6 shows the shock structure close to the TIC nozzle exit at different pressure ratios during a single test run at three time instances. The time interval for each picture is approximately 30 ms. The upper and the lower limits of pressure ratio mentioned in the Figs. 6 give an approximate idea of the pressure ratio at the beginning and end of the each test run and not the precise value for each photograph. The flow is from left to right, with the nozzle exit at the left. In all of the test cases, the length of the first shock cell (defined by the envelop of both oblique shocks emanating from the separation point/nozzle exit and the Mach disk) is seen to decrease with time. This is because, during the test run, the flow exiting from the nozzle into the vacuum tank adds to the initial starting tank pressure. With constant pressure being maintained in the stagnation chamber, the pressure ratio tends to decrease and, hence, results in a change in the flowfield structure with time. Only free-shock separation is observed for all of the test cases, primarily because of the absence of the internal shock in TIC nozzles.[7] At high operating pressure ratios, the separation shock is very close to the nozzle exit, resulting in very long shock cell and a small Mach disk. However, as the pressure ratio decreases (with increasing tank pressure) the shock-cell length is seen to decrease along with the widening of the Mach disk. Figure 6 shows some very interesting flowfield characteristics. Initially (Fig. 6a), a slight asymmetry in the separation flowfield is seen; however, as soon as the pressure ratio drops (Fig. 6b), a relatively greater inclination of the Mach disk appears toward the lower side that increases with decreasing pressure ratio (Fig. 6c), a condition of unsymmetrical-type separation. It has been pointed out by Nave and Coffey[8] that the phenomenon of nozzle separation presents no adverse problem during sea-level operation of an overexpanded nozzle. A problem occurs only when the separation leads to a side load condition. Past investigations have led to the conclusion that the side load problem was associated with an unsymmetrical-type separation, such as the tilted Mach disk case (Figs. 6b and 6c), whereas the dynamic nature of the side loads was due to flow instability.[8] Figure 7 shows another series of schlieren pictures at different pressure ratios. In this case (Fig. 7b), the asymmetry of the Mach disk is opposite to that observed in Fig. 6b [top edge of Mach disk is closer to nozzle exit, relative to those observed in Fig. 6 (lower edge of Mach disk closer to nozzle exit)]. Furthermore, at still lower operating pressure ratios (Fig. 7c), a transition of these two types of asymmetric separation can also be seen. At one instant (Fig. 7b), the top edge of the Mach disk is closer to nozzle exit and at the other (Fig. 7c) the lower edge gets closer, representing a circumferential movement of the leading edge of separation point. The apparent circumferential movement, however, is not of a rotational type, but may be due to the leading edge of separation location oscillating between the two sides of the nozzle. This seems to be a unique feature that possibly could arise from certain flow instability characteristics. No asymmetry was observed for pressure ratios higher than 50 (figures not shown). The preceding observations seem to suggest that 1) asymmetry in flow separation does not occur at all pressure ratios, but only for pressure-ratios less than 45; 2) on the higher side of this range, no circumferential movement of flow asymmetry is seen, whereas on the lower side, the asymmetric separation is observed to exhibit circumferential movement.

According to Dumnov[9] the force acting on the nozzle from the gas flow can be calculated from the following relation,

$$F_{\mathrm{SL}} = \int P_w(x, \phi) R(x, \phi) \cos\phi \, \mathrm{d}\phi \, \mathrm{d}x$$

Even in case of absolute symmetric separation line, random pressure pulsations in the incipient separation zone lead to side load. The key driver is the unsteady component of static pressure and its correlation in the circumferential direction. For an engine operating with a constant combustion chamber pressure, the asymmetry can be split into two parts: an averaged (stationary) one and a pulsating (unsteady) one.[9] The averaged asymmetry or the stationary part can have the following causes: imperfection of burning processes in the combustion chamber, which cause asymmetrical distribution of total pressure and enthalpy along the chamber cross-section, and, therefore, asymmetrical distribution of parameters at the nozzle surface and asymmetrical distortion of the nozzle contour. Such an asymmetry causes, during startup and shutdown, a side load acting on the nozzle and the whole engine. On the other hand, the unsteady part is caused by asymmetrical pulsations like pressure pulsations acting on the nozzle wall and caused by near-wall turbulence.

The flowfield features observed are shown in Fig. 8. If the distance of the Mach disk from 1) the nozzle exit, X_{MD}, and 2) from the nozzle throat, X_{Md}, are measured for different pressure ratios, it is found that this distance vs the pressure ratio follows a particular trend, as shown in Figs. 9a and 9b, similar to that followed by sonic jets. Here, the different symbols in Figs. 9a and 9b represent the different pressure

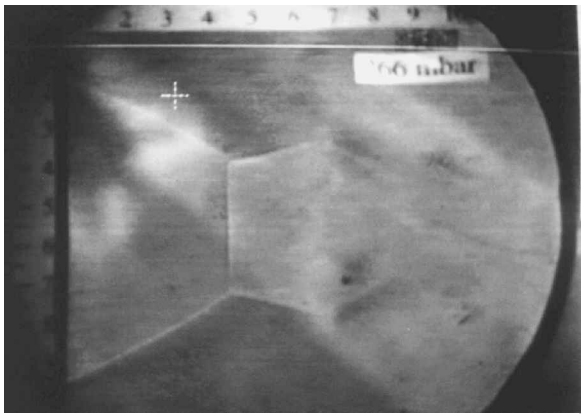

a)

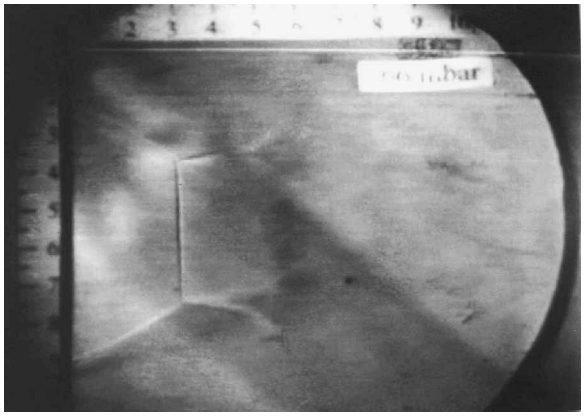

b)

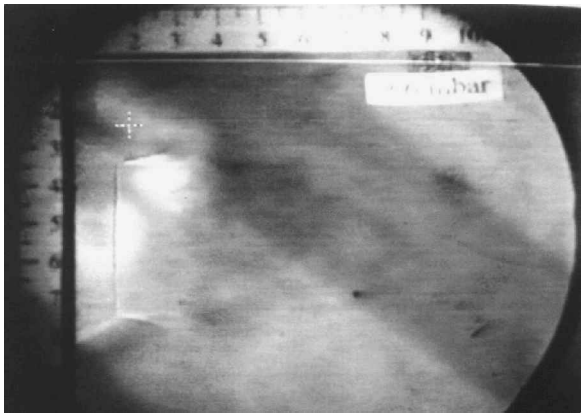

c)

Fig. 7 Schlieren photos of the subscale TIC nozzle during operation at pressure ratio ranging between 45–32 at time instants a) t_1, b) t_2, and c) t_3.

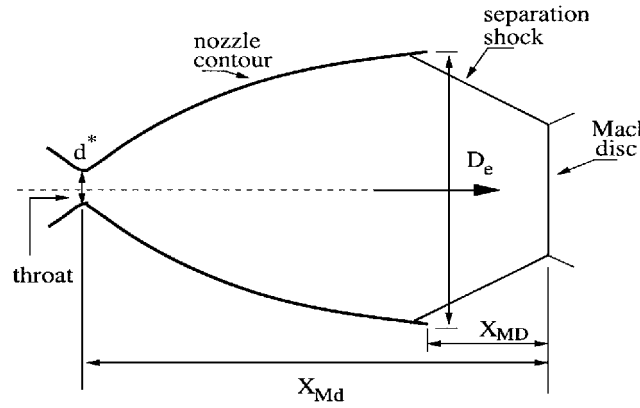

Fig. 8 Flowfield features in overexpanded nozzles.

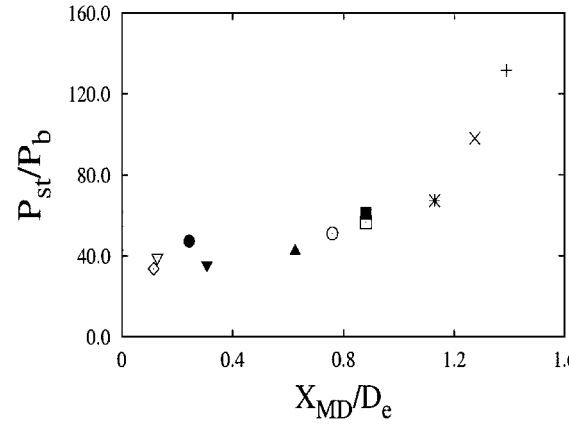

a)

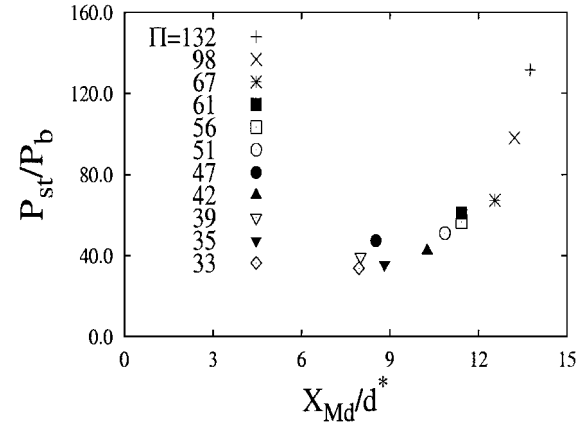

b)

Fig. 9 Variation of Mach disk distance, with nozzle operating pressure ratio: a) X_{MD} nondimensionalized with nozzle exit diameter D_e and b) X_{Md} nondimensionalized with nozzle throat diameter d^*.

ratios for which Mach disk distances were measured. The distance of the Mach disk from the nozzle exit increases with increasing pressure ratio until at higher values; when the separation shock is close to the nozzle exit, the trend approaches an asymptotic value.

Wall Pressure Distribution

Because of limitations of charge tube pressure of 80 bar, nozzle pressure ratios above 30 could not be achieved with the vacuum tank open to atmosphere. For pressure ratios above 30 that tank had to be closed and the pressure inside it controlled. Although this enabled a range of pressure ratios during a single test run, it did not, however, allow for steady-state conditions because the vacuum tank pressures would increase during a test run. Nine separate transducers were mounted flush on the nozzle contour, their signals being simultaneously sampled and recorded. Two pressure sensors were also mounted at a circumferential angle of 180 deg to the initial position of transducers as shown in Fig. 10 (numbers 3 and 5 and 8 and 9). This was primarily done to record any asymmetry of flow separation inside the nozzle during operation at different time instances. The diameter of the pressure taps is 0.5 mm, and they were drilled vertically (as indicated in the Fig. 10) into the wall.

Figure 11 shows the measured wall pressure distribution over a range of pressure ratios. Here the wall pressure P_w is nondimensionalized by the back pressure P_b, and the nozzle axial distance X is nondimensionalized by the nozzle throat radius r_t. At a high pressure ratio of 83, the flow is observed to expand toward the end of the nozzle, which is due to the increasing Mach number. However, at a pressure ratio of 47, Fig. 11 shows a separation point, marked by a sudden increase in wall pressure close to nozzle exit. At lower pressure ratios, as expected, the separation point continues to move

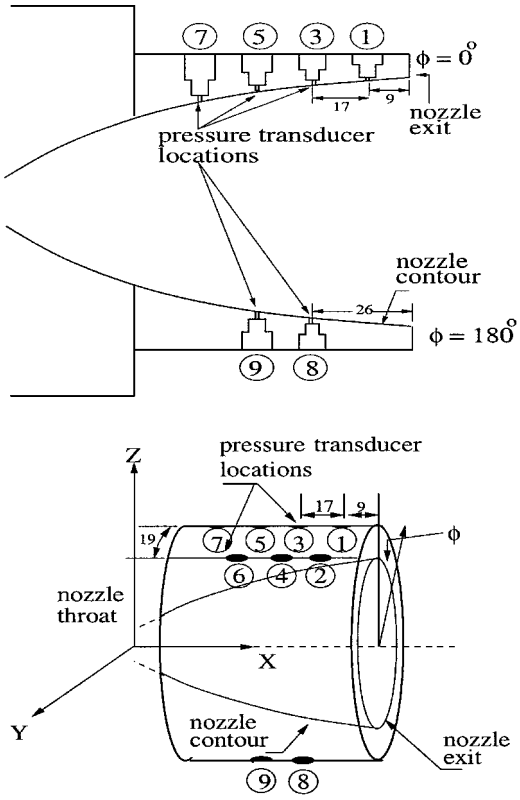

Fig. 10 Arrangement of pressure transducers on the nozzle contour for the study of flow separation, all dimensions in millimeters.

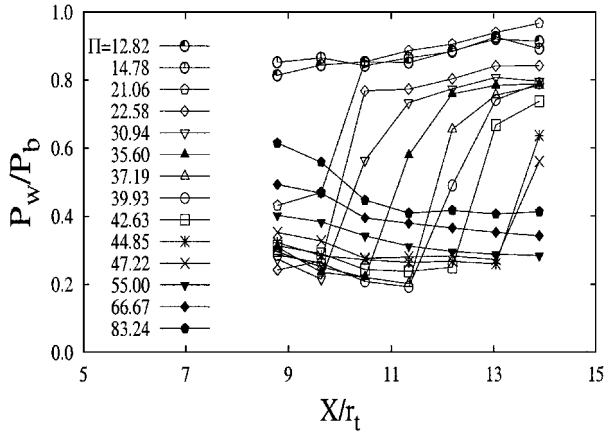

Fig. 11 Wall pressure distribution inside the TIC nozzle at pressure ratios up to 84.

upstream further inside the nozzle so that a near-constant plateau of pressure in the recirculation region, after separation, can be seen. However, the pressure in the recirculation region stays clearly below 1.0 and in the range of 0.8–0.95. This is caused by the long narrow geometry of the nozzle. Such wall pressure distribution is typical to free-shock separation (FSS) where the separated flow continues as a freejet (Fig. 5). For separation close to the nozzle exit, there is an effect noted in literature[8] that the pressure rise downstream of the separation can be markedly less than when the shock is well inside the nozzle. This is sometimes called the "separation end effects." The data shown in Fig. 11 for pressure ratios in the range of 39.93–47.22 show this characteristic, in that the pressure rise for separation close to the nozzle exit is less than the rise noted at lower pressure ratios.

Figure 12a is a representation of the wall pressure variation encountered by each pressure transducer over the range of pressure

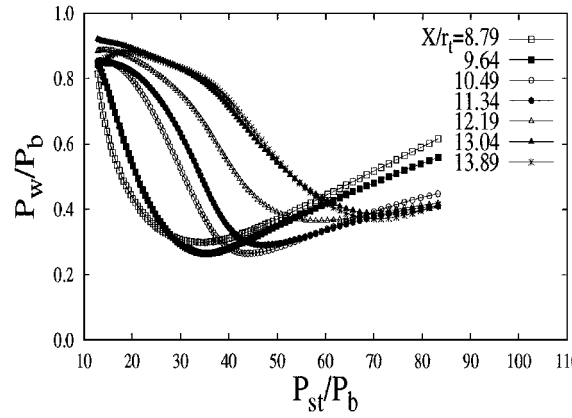

Fig. 12a Variation of wall pressure at different axial location over a range of operating pressure-ratios.

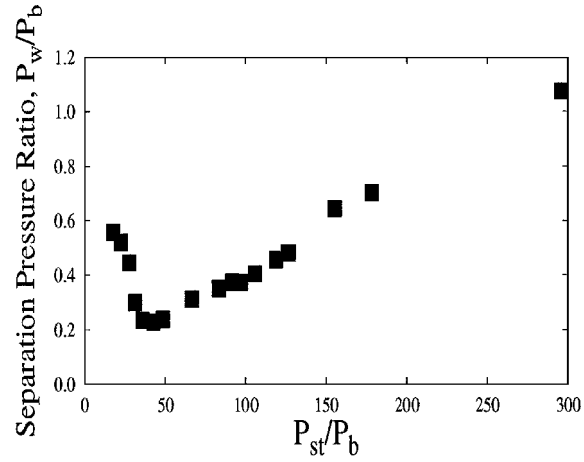

Fig. 12b Separation end effects.

ratios tested. It can be seen for all of the cases that as the pressure ratio is increased, the wall pressure inside shows a considerable decrease before finally showing a rise at higher pressure ratios. The points way inside the nozzle show a sharper fall and rise relative to points close to nozzle exit. Figure 12b shows the variation of separation pressure ratio over the range of nozzle pressure ratios carried out. The wall pressure P_w here corresponds to the pressure at the beginning of separation (the point from which the wall pressure rise is observed) at each nozzle pressure ratio. This value of P_w is then nondimensionalized by the corresponding local back pressure P_b for each case. For pressure ratios at which the separation shock is at the nozzle exit, the wall pressure from the transducer closest to the nozzle exit, is taken. It would appear that in the limit, an expansion nozzle of high area ratio will not flow fully until the wall pressure at the exit obtains a value of the local back pressure.

Though it is known[10] that in reality there is no exact point of separation because it fluctuates between two extreme locations, much experimental data have been used in the past to develop theoretical predictions of FSS. Figure 13 shows the comparison of the experimental data points with that developed by Schmucker (see Ref. 2). Though Schmucker's criteria gives the correct trend for the Mach number dependence of flow separation, a significant scatter of the data points around the curve is observed. Frey[11] and Hagemann et al.[10] suggest that some important parameters such a nozzle contour, temperature influence, wall roughness, and gas properties that significantly effect the separation behavior need to be addressed in the prediction criteria.

One of the contour parameters that seem to influence the flow separation behavior was pointed out by Hagemann et al.[10] to be the radial size of the recirculation zone between the nozzle wall and the jet, which can be approximated by the difference between the total area ratio and the area ratio at the separation point, $\epsilon - \epsilon_{sep}$. Figure 13b shows the influence of this parameter on the pressure

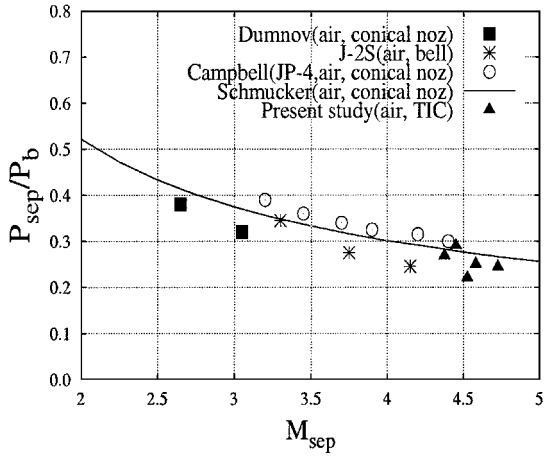

Fig. 13a Experimental free-shock separation data compared to Schmucker's criterion (see Ref 2).

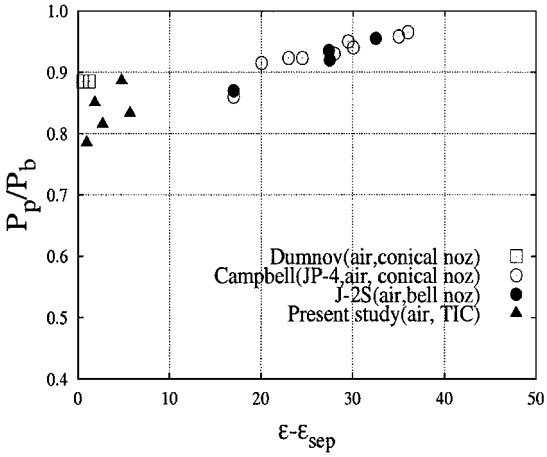

Fig. 13b Dependence of the pressure increase in the recirculation zone on the contour and the location of separation point.

recovery in the separated region. It can be discerned from the previous and present study that the smaller the radial size of recirculation zone (i.e., for separation near nozzle exit), the stronger the rise of plateau pressure to ambient pressure in the recirculation zone and vice versa.

To study the time-dependent nature of separation shock, it is necessary to plot the instantaneous wall pressure distributions during a single test campaign. Figure 14 shows the instantaneous wall pressure distribution as a function of time vs X/r_t. The results shown correspond to the test campaign for which the schlieren pictures are shown in Fig. 7. In Figs. 14b and 14d, the plot shows a slight asymmetry in the point of separation observed for pressure taps located at circumferential angle of 180 deg, but similar axial locations. Because the stagnation chamber pressure shows steady conditions (figure not shown) during the test run, the wall distribution, therefore, indicates some transient phenomena that seems to result in the asymmetry. Also note that the flow asymmetry shifts circumferentially at different time intervals, as was also seen in the schlieren pictures of Figs. 7b and 7c, resulting in a tilted separation plane that may contribute to nozzle side loads. Such a circumferential flow asymmetry was not only observed for the case shown in Fig. 14, but was also observed for other nozzle pressure ratios (figures not shown) ranging between 30 and 42. It has, however, been pointed out by Nave and Coffey[8] that the origin of dynamic side loads is a result of pressure pulsations in the separated/reattachment regions and not an unsymmetrical flow separation. This behavior was also observed. At a pressure ratio of 21 (the steady pressure ratio condition), a very interesting feature was observed (Fig. 15). At certain time instances (Figs. 15a–15c) the separation point is observed to move considerably over the length of the nozzle. It is certain that

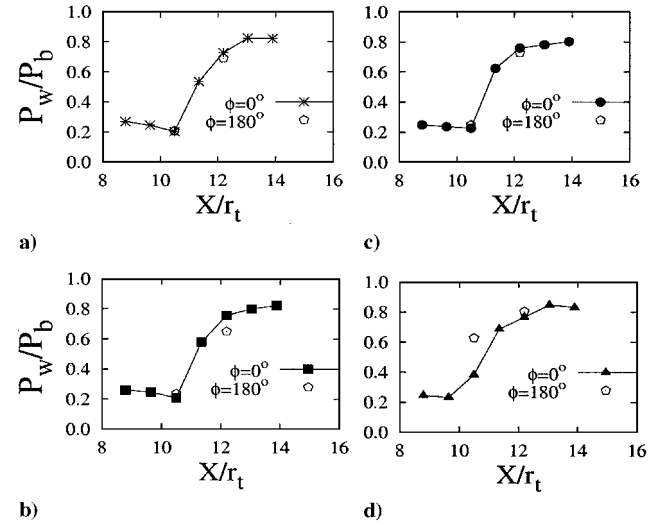

Fig. 14 Wall pressure distribution inside the TIC nozzle at different time instances, Π= 32: a) 80, b) 90, c) 100, and d) 110 ms.

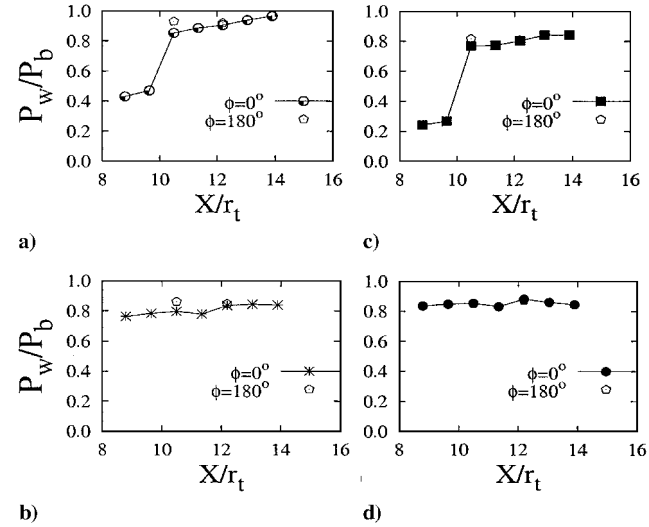

Fig. 15 Wall pressure distribution inside the TIC nozzle at different time instances, Π= 21.06: a) 50, b) 60, c) 70, and d) 80 ms.

the flow is very unstable in this pressure ratio range. Some similar behavior was also observed for pressure ratios of 12–14 (figures not shown). According to Nave and Coffey,[8] the separation and side load characteristics of the small-scale models are similar to those observed on the full-scale hardware. Although size may change the absolute value of the side load and separation characteristics, the mechanisms that produce those characteristics are the same.

In summary, therefore, the schlieren pictures indicate the existence of asymmetric flow separation in the FSS category. Furthermore, two distinct flowfield features could be observed from the wall pressure distributions. First, at very low pressure ratios, the flow inside the nozzle is unstable, showing a considerable movement of separation point. Second, between pressure ratios of 32 and 45, the separation exhibits asymmetry over the circumference of the nozzle geometry, which may, in principle, result in side loads. The reversal of asymmetric separation along the nozzle circumference, as observed in the schlieren photographs (Fig. 7) could not be seen in the wall pressure distribution plots. These observations, however, are of considerable importance and require further detailed investigations.

Fluctuating Wall Pressure Signal

Kistler, in 1964, was probably the first to make quantitative measurements and to document the character of the wall pressure signal $P_w(t)$ near separation.[12] A typical pressure signal measured upstream of separation, which has all of the features observed by

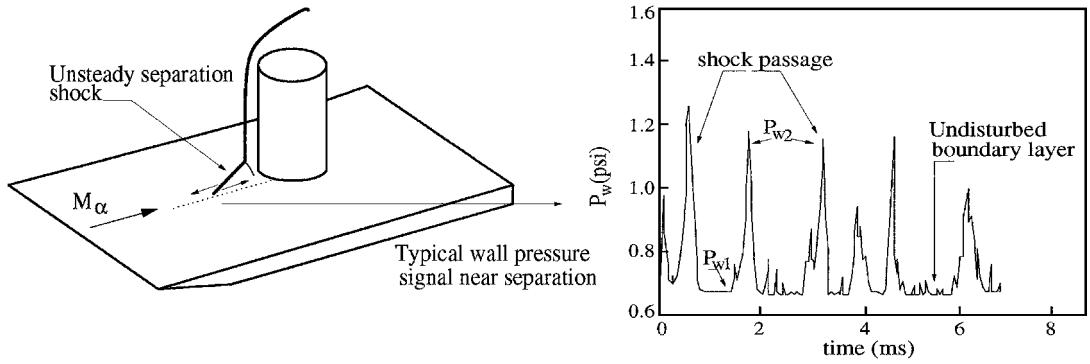

Fig. 16 Typical intermittent wall pressure signal near separation.[13]

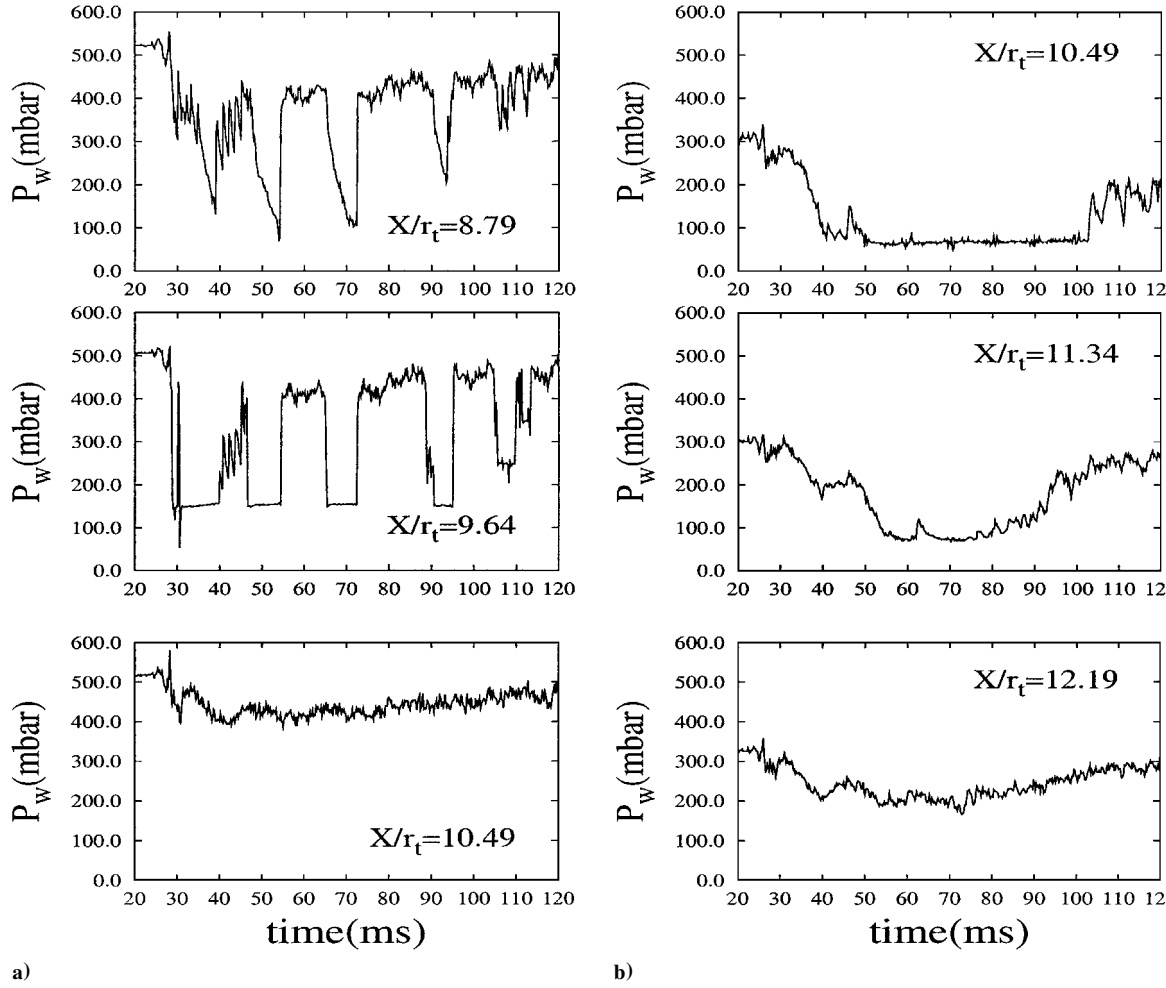

Fig. 17 Instantaneous wall pressure signal for transducer locations showing movement of separation shock: a) Π= 21.06 and b) Π= 35.60.

Kistler, but from the study carried out by Dolling and Narlo[13] for separated flow induced by a unswept circular cylinder on a flat plate, is shown in Fig. 16. Note that the moving separation shock generates an intermittent wall pressure signal $P_w(t)$ whose level fluctuates between the range characteristic of the undisturbed turbulent boundary layer and that of the disturbed flow downstream of the shock. Evidence suggests that the instantaneous separation point and shock foot are essentially at the same location and that the separation line is the downstream boundary of a region of intermittent separation.[13] Since Kistler's work, pressure signals such as these have been measured in a wide variety of interactive flows at speeds from transonic to hypersonic.[14–18] These dynamic wall pressure measurements, shown in Fig. 16, indicate clearly that the separation shock shows a large-scale streamwise oscillatory motion or "flapping" of the shock wave across the location of the wall pressure measurement. The signals show a highly intermittent nature and are seen to jump between two levels, indicated by P_{w1} (lower level) and a high level marked as P_{w2} in Fig. 16. P_{w1} is pressure signal measured when the "foot" of the shock wave was downstream of this transducer, whereas P_{w2} was measured when the shock was upstream of this transducer.

A similar type of pressure signal is observed in the present study of the flow separation in the TIC nozzle. Figure 17a shows the wall pressure signals from the transducers that experience such a fluctuating signal (pressure ratio 21, Fig. 15). This type of oscillatory pressure signal was observed only for pressure ratios of 21 and below and not for higher values (Fig. 17b) where, it seems, the flow is considerably stabilized with little or no movement of separation shock. The latter part of the preceding statement needs further experimental scrutiny with closely spaced transducer locations along the nozzle

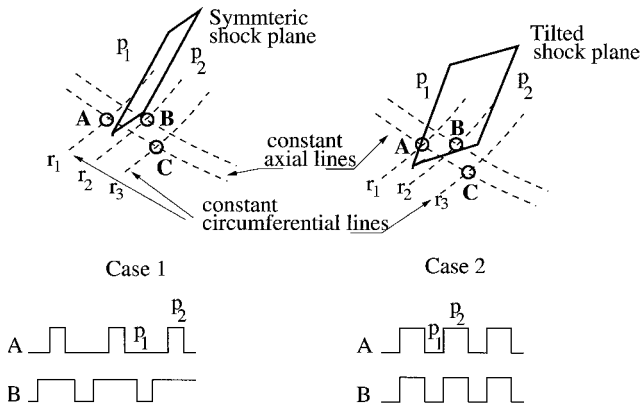

Fig. 18 Schematic of the separation shock plane movement as visualized from the transducer signals.

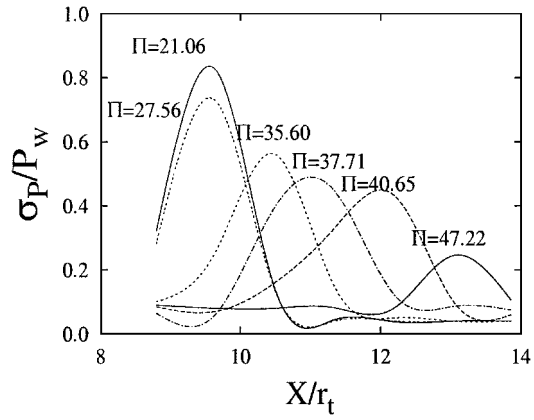

Fig. 19a Distribution of rms vs axial length as a function of nozzle pressure ratio.

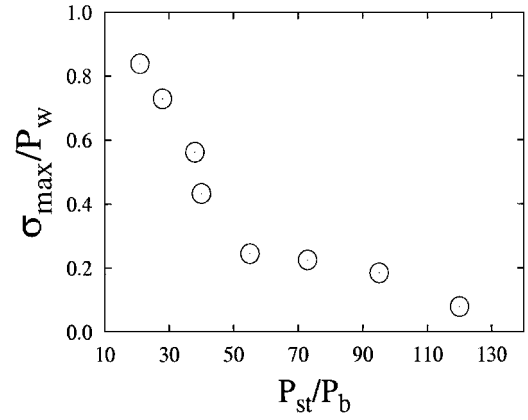

Fig. 19b Maximum rms vs nozzle pressure ratio.

length. This is because, in our case, the transducers were placed 8.5 mm apart axially and might have missed the separation shock fluctuations, which seem to be much smaller with increasing pressure ratios, that is, with the separation location moving toward the nozzle exit. This is somewhat highlighted in the rms plots discussed later. In other words, therefore, the large-scale oscillatory motion of the separation shock in nozzle flows seems to be influenced strongly by the curvature of the divergent section of the nozzle.

Furthermore, it is worth pointing out here that though the pressure signals shown in Fig. 17a are from transducers placed in streamwise direction, these transducers are not placed in the same axial line, as was also shown in Fig. 10 (locations 5, 6, and 7). Here, in Fig. 17a, the transducers at $X/r_t = 8.79$ and 10.49 are in the same axial line, the one at $X/r_t = 9.64$ is midway between the aforementioned two, but 19 mm away laterally. That the transducers placed laterally and at different axial locations show a shock flapping in the same time period suggests that the separation location was not circumferentially symmetric. From this we can conclude that the separation at the measurement location was tilted. This locally tilted separation could induce asymmetric shock patterns as seen in the schlieren photographs. Figure 18 clarifies the preceding statement. Note that if the shock plane is symmetrical (circumferentially) (case 1) then, while oscillating between transducers A and B at some time instant, it will be in between the two. At this time, A will show lower pressure and B higher (being behind the separation shock). When the shock plane is ahead of A then both A and B show higher pressure levels, and when it is behind B then both A and B show lower pressure levels. The type of pressure signals that A and B will generate under such a symmetrical shock plane oscillation is as shown in case 1 (lower part). However, such a type of pressure signal was not obtained from the present test results. Rather, the pressure level was observed to fluctuate up and down at the same time instants, hinting that the shock plane crosses transducers A and B at the time instants. Case 2 in Fig. 18 shows this. Because, in our case, the transducers A and B are not in the same axial line and are spaced laterally (in a zig-zag fashion), such a pressure signal suggests the separation shock to be tilted while oscillating at this pressure ratio. The angle of the tilt being determined by the angle between A and B relative to the circumferential line at either A or B, which turns out to be 24.10 deg in our case. This does not, however, imply that the separation line is tilted at 24.10 deg all of the way around the nozzle, but just the local separation line that may be due to the "tepees" of separation. Such tepees have been observed by Nave and Coffey[8] in the video and still images of nozzle separation tests with the camera looking up into the nozzle. The phenomena shown in Fig. 17a was repeatable and was observed for all test conditions corresponding to low nozzle pressure ratios between 12–21. At these low pressure ratios, the exhaust flow containing the first shock cell is way inside the nozzle and, therefore, prevents visualization of the first shock cell, making it difficult to correlate the preceding phenomena with tilted Mach disk from the same test runs.

The separation, therefore, at low pressure ratios, exhibits both asymmetry and oscillatory movement that can result in significant side loads.

RMS Distributions

Figure 19a shows the streamwise distributions of the nondimensionalized rms wall pressure fluctuations σ/P_w as a function of nozzle pressure ratio. In all of the cases, the distributions show a peak in rms value occurring ahead of ahead of separation.[19] A large increase of σ_{pw} has been pointed out by Andreopoulos et al.[19] and Garg and Settles[20] to be due to the intermittent nature of the pressure fluctuations caused by the back and forth motion of separation shock. Aft of the separation peak, the rms level in Fig. 19a is observed to drop and remain relatively constant for the remaining axial length. This region approximately corresponds to the so-called plateau region in the wall pressure distribution plot. Also note that the peak in rms is the maximum for a pressure ratio of 21 and tends to decrease with increasing pressure ratio. The rms levels for pressure ratios below 21 could not be shown because the design limits of the nozzle fabrication did not allow the transducers to be mounted for $X/r_t < 8.49$. This is seen in Fig. 19b, which shows the distribution of maximum rms as a function of nozzle pressure ratio.

It is clear then, that the intermittent nature of the separation shock is strongly governed by the axial location of separation and, hence, on the curvature of the nozzle. The greater the local wall curvature is the higher the fluctuation intensity is. This may directly contribute to the side loads at low pressure ratios inherit to the transient startup and shutdown of TIC nozzles.

Conclusions

An experimental investigation has been conducted to study the separation characteristics in a TIC nozzle. Schlieren visualizations reveal the existence of the tilted Mach disk for pressure ratios below

45. Furthermore, a switch from symmetrical to asymmetrical type of separation is observed as the pressure ratio decreases during a test campaign. Another test campaign reveals circumferential movement of the Mach disk. Pressure signals in the vicinity of separation show the moving separation shock to generate an intermittent wall pressure signal. Furthermore, the placement of pressure transducers reveal this oscillating shock to be tilted. Such an asymmetry, combined with intermittent pressure pulsations, can cause, during startup and shutdown, side loads acting on the nozzle and the whole engine.

The analysis of the unsteady wall pressure measurements shows that the pressure rms levels reach a maximum in the shock wave/boundary-layer interaction region of separation. It is also seen that the separation shock unsteadiness decreases with increasing pressure ratio, indicating that the separation characteristics are very sensitive to the location inside the overexpanded nozzle and that the nozzle contour is a strong parameter governing the separation shock oscillations.

Acknowledgment

This study was carried out as a part of the research work under the Alexander von Humboldt fellowship at Hyperschall Technologie Göttingen (HTG), Katlenburg-Lindau, Germany between July 1999 and Feb. 2001. The author would like to thank the foundation and HTG for the same.

References

[1]Rao, G. V. R.,"A Review of Rocket Nozzle Configuration," ESA, Noordwijk, Netherlands, 1992, pp. 1–8.

[2]Frey, M., and Hagemann, G.,"Restricted Shock Separation in Rocket Nozzles," *Journal of Propulsion and Power*, Vol. 16, No. 3, 2000, pp. 478–484.

[3]Romine, G. L., "Nozzle Flow Separation," *AIAA Journal*, Vol. 36, No. 9, 1993, pp. 1618–1625.

[4]Hoegman, U., Mattsson, J., and Torngren, L.,"A Sub-Scale Test Programme on Investigation of Flow Separation and Side-Loads in Rocket Nozzles," *Proceedings of the 3rd European Symposium on Aerothermodynamics of Space Vehicles*, ESA–ESTEC, Noordwijk, The Netherlands, 1998, pp. 373–378.

[5]Koppenwallner, G., Friehmelt, H., and Muller-Eigner, R., "Calibration and First Results of Redesigned Ludwieg Expansion Tube," AIAA Paper 93-5001, Nov–Dec. 1993.

[6]Foster, C., Summerfield, M., and Swan, W., "Flow Separation in Overexpanded Supersonic Exhaust Nozzles," *Jet Propulsion*, Vol. 24, No. 9, 1954, pp. 319–321.

[7]Stark, R., Ciezki, H. K., Quessard, F., Frey, M., and Kwan, W., "Subscale Nozzle Testing at the P6.2 Test Stand," AIAA Paper 2000-3777, 2000.

[8]Nave, L. H., and Coffey, G. A., "Sea-Level Side Loads in High-Area-Ratio Rocket Engines," AIAA Paper 73-1284, 1973.

[9]Dumnov, G. E., "Unsteady Side Loads Acting on the Nozzle with Developed Separation Zone," AIAA Paper 96-3220, July 1996.

[10]Hagemann, G., Terhardt, M., and Frey, M., "Flow Separation and Side-Load Behavior of Truncated Ideal Rocket Nozzles," AIAA Paper 2001-3686, 2001.

[11]Frey, M., "Shock Patterns in the Exhaust Plume of Rocket Nozzles," *Proceedings of the 3rd European Symposium on Aerothermodynamics of Space Vehicles*, ESA–ESTEC, Noordwijk, The Netherlands, 1998, pp. 395–403.

[12]Kistler, A. L., "Fluctuating Wall Pressure Under a Separated Supersonic Flow," *Journal of the Acoustical Society of America*, Vol. 36, No. 3, 1964, pp. 543–550.

[13]Dolling, D. S., and Narlo, J. C., II, "Driving Mechanism of Unsteady Separation Shock Motion in Hypersonic Interactive Flow," *Aerodynamics of Hypersonic Lifting Vehicles*, CP-428, AGARD, 1987, pp. 7-1–7-12.

[14]Dolling, D. S., and Murphy, M. T., "Unsteadiness of the Separation Shock Wave Structure in a Supersonic Compression Ramp Field," *AIAA Journal*, Vol. 21, No. 12, 1983, pp. 1628–1634.

[15]Dolling, D. S., and Brusniak, L., "Separation Shock Motion in Fin, Cylinder, and Compression Ramp Induced Turbulent Interactions," *AIAA Journal*, Vol. 27, No. 6, 1989, pp. 734–742.

[16]Dolling, D. S., "Unsteadiness of Supersonic and Hypersonic Shock-Induced Turbulent Boundary-Layer Separation," Rept. 764, AGARD, 1990, pp. 7-1–7-26.

[17]Tran, T. T., Tan, D. K. M., and Bogdonoff, S. M., "Wall Pressure Fluctuations in a Three-Dimensional Shock Wave/Turbulent Boundary-Layer Interaction," *AIAA Journal*, Vol. 25, No. 1, 1987, pp. 14–21.

[18]Dussauge, J. P., Muck, K. C., and Bogdonoff, S. M., "Structure of Wall Pressure Fluctuations in a Shock-Induced Separated Turbulent Flow," AIAA Paper 85-0179, 1985.

[19]Andreopoulos, J., Muck, K., and Dussauge, J., "Unsteady Nature of Shock Wave/Turbulent Boundary-Layer Interaction," *AIAA Journal*, Vol. 26, No. 2, 1988, pp. 179–187.

[20]Garg, S., and Settles, G. S., "Unsteady Pressure Loads Generated by Swept Shock Wave/Boundary-Layer Interactions," *AIAA Journal*, Vol. 34, No. 6, 1996, pp. 1174–1181.